Preprints of the 21st IFAC World Congress (Virtual)
Berlin, Germany, July 12-17, 2020

# Multi-layer Predictive Energy Management System for Battery Electric Vehicles

**Róbinson Medina, Zjelko Parfant, Thinh Pham, and Steven Wilkins** *

* *Automotive Campus 30, 5708 JZ Helmond. TNO powertrains. (e-mail: robinson.medina@tno.nl).*

**Abstract:** Range anxiety is one of the barriers for the customer acceptance of Battery Electric Vehicles (BEVs). To cope with this limitation, this paper presents a Predictive Energy Management System (PEMS) that can reduce total battery energy consumption by using available up-coming route information such as traffic flow, speed limits and road slope. The developed PEMS contains two optimization layers: the first layer generates a speed profile for the upcoming route that minimizes driving energy, while simultaneously controlling the average driving speed; the second layer reduces the energy consumption of the Heating, Ventilation, and Air Conditioning (HVAC) system, while guaranteeing driver thermal comfort. The proposed PEMS results in an algorithm capable of running in real time, due to the use of simplified vehicle and powertrain component models. Simulation results show potential energy savings of 7.1% compared to a baseline strategy, i.e. a non-predictive energy management system.

*Keywords:* dynamic programming, energy management systems, electric vehicles, optimal control, supervisory control, speed control, temperature control.

## 1. INTRODUCTION

The use of vehicles based on petroleum fuel has been predominant for the last century. However, due to the negative environmental impact and depletion of petrol resources, alternatives such as Battery Electric Vehicles (BEVs) are regarded as promising solutions for reducing fuel dependency, see Onat (2015). BEVs use electricity as energy source which results in zero tank-to-wheel emissions. However, one of the main limiting factors for its widespread adoption is the range anxiety that results from constraints in the amount of energy that can be stored in high-voltage batteries, see Egbue and Long (2012).

Efforts to increase the BEVs range include improving the efficiency of either the hardware or the software used in the powertrain. Improving the hardware focuses on enhancing the efficiency of the vehicle components (e.g. battery packs, power electronics, and so on). For example, de Santiago et al. (2012) shows an overview of different Electric Machines technologies. Improving the software focuses on improving the Energy Management System (EMS) from particular components or from the vehicle as a whole. An example of improved EMS for components, is the Battery Management System presented by Cao et al. (2008), which enhances battery efficiency. Another example is the Predictive Energy Management System (PEMS) of the Heating, Ventilation, and Air Conditioning (HVAC) system of Schaut and Sawodny (2019), which enhances the thermal system efficiency; an example of improved EMS of the vehicle as a whole is the predictive EMSs of Morlock et al. (2017), which uses road profile to minimize powertrain energy. This paper focuses on predictive EMSs for the entire vehicle, including the thermal system.

Model predictive control is a commonly used supervisory control strategy since it allows to minimize power-related cost functions, while guaranteeing compliance to a set of constraints. For example, a PEMS for the whole vehicle that generates a speed profile is presented by Morlock et al. (2017) and Yan et al. (2014). Morlock et al. (2017) showed that this EMS can reduce energy losses up to 28% with "aggressive" drivers. These EMSs use road profile information and multiple driver profiles to generate a driving strategy that reduces power energy in the electric powertrain. Another example of predictive EMSs was presented by Eckstein et al. (2016b,a), which focuses on reducing the energy consumption of the HVAC. Reducing the energy consumption of the HVAC is a relevant objective, since the HVAC can reduce the range of a passenger BEV from 17% to 37% in summer time, as reported by Zhang et al. (2017). The predictive EMSs of Eckstein et al. (2016b,a) use road information to determine when and how to optimally use the HVAC, such that energy savings are maximized while passengers' thermal comfort is guaranteed.
All of these EMSs have a single optimized variable: either longitudinal vehicle speed or HVAC energy. Combining the benefits of both speed and HVAC power optimization in a single EMS has not been explored before.

**Contributions** This paper presents a multi-layer Predictive Energy Management System (PEMS) for a BEV, which consists of two optimization layers. The first layer generates a speed profile that minimizes driving energy, while controlling the average driving speed. Savings are achieved by exploiting knowledge of the road profile, speed limits, and traffic conditions, to minimize powertrain losses. The second layer uses the generated speed profile

⋆ The findings of this paper were obtained within the European project HiFi-ELEMENTS.

from the first layer to determine the optimal power flow to the HVAC that minimizes the total battery energy consumption, while guaranteeing thermal comfort for the driver. The proposed PEMS uses simplified models of the vehicle and the powertrain components, which results in an algorithm capable of running in real time. .

This paper is divided as follows. Section 2 introduces the simplified vehicle and component models. These simplified models are used in Section 3 to design the multi-layer PEMS. Simulation results are presented and analysed in Section 4. Conclusions are given in Section 5.

## 2. VEHICLE AND POWERTRAIN MODEL

In this section, the simplified vehicle and component models that are used by the multi-layer PEMS are presented.

### *2.1 Vehicle model*

The longitudinal dynamics of the vehicle are described with a single first-order differential equation, which is taken from (Guzzella et al., 2007, Chapter 2):

$$m\dot{V}_x = F_x - F_{drag} - mg(sin\alpha + c_{rr}cos\alpha), \quad (1)$$

where $F_{drag}$ $[N]$ the force due to air drag, $V_x$ $[m/s]$ is the longitudinal speed, $F_x$ $[N]$ is the force applied at the wheels, and $\alpha$ $[rads]$ is the road slope. The air drag is further defined as:

$$F_{drag} = \frac{1}{2}C_d A V_x^2. \quad (2)$$

The model coefficients are described in Table 2.

### *2.2 Powertrain component models*

The electric energy consumption is calculated from the power at the wheel $P_{wh}[w]$ and the thermal system $P_{HVAC}$, based on the powertrain topology shown in Fig 1. Here, a High-Voltage Battery (HVB) supplies power to a thermal system and the vehicle power train, i.e. high-voltage DC/DC converter, a motor Inverter (INV), an Electric Motor (EM), and a fixed-gear transmission (TM). The powertrain components are described in Pham et al. (2016). The models are summarized in Table 1. These

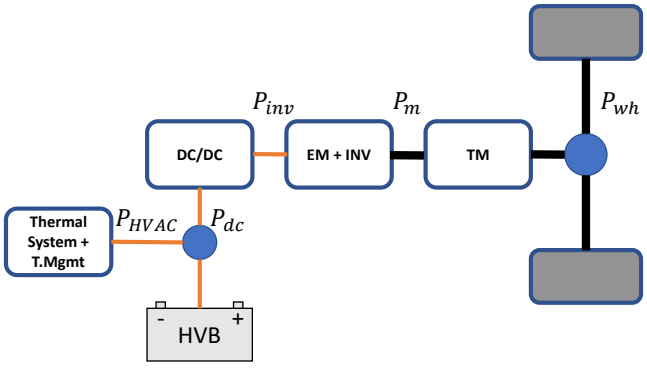


Fig. 1. Powertrain topology. The powertrain consists of a High-Voltage Battery (HVB), a high voltage DC/DC converter (DC/DC), an Electric Machine with an Inverter (EM+INV), and a Transmission (TM).

Table 1. Powertrain models.

| **Component power** $[W]$ | **Equation** |
|---|---|
| Wheel | $P_{wh} = F_x V_x$ |
| Motor output | $P_m = \frac{P_{wh}}{\eta_{trans}}$ $\forall P_{wh} > 0$<br>$P_m = P_{wh}\eta_{trans}$ $\forall P_{wh} < 0$ |
| Inverter input | $P_{inv} = \frac{(1-\alpha_1)-\sqrt{(\alpha_1-1)^2-4\alpha_2(\alpha_0+P_m)}}{2\alpha_2}$ |
| DC/DC input | $P_{dc} = \frac{P_{inv}}{\eta_{dc}}$ $\forall P_{dc} > 0$<br>$P_{dc} = P_{inv}\eta_{dc}$ $\forall P_{dc} < 0$ |
| Battery terminal | $P_s = P_{dc} + P_{HVAC}$ |
| Battery stored | $P_{batt} = \frac{1-\sqrt{1-4\beta_0(P_s)}}{2\beta_0}$ |
| HVAC input | $P_{HVAC} = \frac{\dot{Q}_{inlet}}{CoP^+}$ $\forall \dot{Q}_{inlet} > 0$<br>$P_{HVAC} = \frac{\dot{Q}_{inlet}}{CoP^-}$ $\forall \dot{Q}_{inlet} < 0$ |

models range from constant efficiency to quadratic relations between input and output power. Note that the sign convention is chosen such that a power flow that discharges the battery is defined as positive. The thermal model is further detailed in Section 2.3. Model parameters used for the both the vehicle and thermal model are shown in Table 2.

### *2.3 HVAC model*

The magnitude of the HVAC power depends on the input cabin heat flow $\dot{Q}_{inlet}$ $[J]$, as defined below:

$$\dot{Q}_{inlet} = C_p \rho \dot{m}(T_{inlet} - T_{cab}),$$

where $\dot{m}$ $[kg/s]$ is the (fixed) mass flow of the air inlet, and $T_{cab}$ $[K]$ and $T_{inlet}$ $[K]$ are the cabin and inlet temperatures respectively.

The simplified cabin thermal system is given by:

$$C_{th}\dot{T}_{cab} = \frac{(T_{amb} - T_{cab})}{R_{th}} + \dot{Q}_{inlet} + K_{sun}E_{sun} + K_{pas}N_{pas}, \quad (3)$$

with $T_{amb}$ $[K]$ is the ambient temperature. The thermal model parameters are defined in Table 2.

## 3. MULTI-LAYER ENERGY MANAGEMENT STRATEGY

This section presents the formulation of the PEMS consisting of two layers: one for speed profile and one for HVAC power. Each layer requires an optimization algorithm. Dynamic Programming (DP) is selected as method to solve these optimization problems, since this method can find the global optimum for any (nonlinear) optimal control problem, provided that the discretization grid is chosen correctly. However, this method typically faces a trade-off between optimality and computational demand, since its computational cost increases exponentially with the number of states of the dynamic model (see Guzzella et al. (2007)).

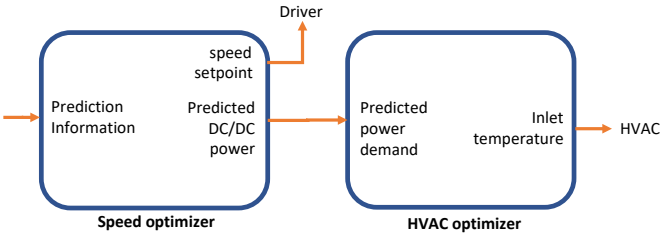


Fig. 2. Schematic overview of the multi-layer PEMS.

To keep the computational cost to a minimum, the optimal control problem, consisting of finding optimal HVAC power and optimal speed profile is separated into two single-state optimization problems, which are solved sequentially. For this reason, it can be seen as a multi-layer energy management strategy. In the case of passenger cars, this approach will not significantly affect the optimality of the found solution, since the HVAC power flows are relatively small as compared to the power flows resulting from driving the vehicle. At each time-step, the control problem of finding the optimal speed profile is solved first, since the HVAC control problem needs the predicted input power flow to the DC/DC converter $P_{dc}$. A schematic overview of the proposed optimization algorithm is shown in Figure 2.

### *3.1 Speed profile optimization*

The vehicle speed profile optimization seeks to minimize total battery energy consumption, which is related to vehicle speed $V_x$ and tractive force $F_x$ as shown in differential Eq. 1 and Table 1. Although Eq. 1 is time-based, distance-based prediction is preferred since the speed constraints

Table 2. Model parameters.

| | **description** | value | units |
|---|---|---|---|
| **Vehicle parameters** | | | |
| $m$ | vehicle mass | 2000 | $kg$ |
| $c_{rr}$ | rolling resistance | 0.006 | – |
| $C_dA$ | Air drag and frontal area coefficient | 0.6 | $kg/m$ |
| **Powertrain parameters** | | | |
| $\eta_{trans}$ | transmission efficiency | 0.98 | – |
| $\alpha_2$ | EM coefficient | $5.6 \times 10^{-7}$ | $1/W$ |
| $\alpha_1$ | EM coefficient | $-43\times10^{-4}$ | – |
| $\alpha_0$ | EM coefficient | 785 | $W$ |
| $\eta_{dc}$ | DC/DC converter efficiency | 0.99 | – |
| $\beta_0$ | battery power loss coefficient | $41 \times 10^{-7}$ | $1/W$ |
| $CoP^+$ | heating coefficient of performance | 2.14 | – |
| $CoP^-$ | cooling coefficient of performance | -2.14 | – |
| **Thermal parameters** | | | |
| $C_{th}$ | thermal capacitance | $113 \times 10^3$ | $J/K$ |
| $C_p$ | specific heat | 1000 | $J/Kg$ |
| $R_{th}$ | thermal resistance | $15 \times 10^{-6}$ | $K/J$ |
| $E_{sun}$ | sun Irradiance | 265 | $W/m^2$ |
| $K_{sun}$ | Irradiance area | 1.77 | $m^2$ |
| $K_{pas}$ | passenger metabolism | 104 | $W$ |
| $N_{pas}$ | Number of passengers | 4 | – |

(e.g. legal speed limit) depend on the location of the vehicle rather than time.

To derive a distance-based prediction model, Eq. 1 is discretized as:

$$m\frac{\Delta V_x}{\Delta t} = F_x - \bar{F}_{drag} - mg(sin\alpha + c_{rr}cos\alpha), \quad (4)$$

where $\bar{F}_{drag}$ $[N]$ is the average air drag force during the discretization interval, $\Delta V_x$ $[m/s]$ is the discrete-time approximation of the change in vehicle speed, and $\Delta t$ $[s]$ is the time interval needed to move one step in the prediction. The speed increase is further defined as

$$\Delta V_x = V_x - V_x(0), \quad (5)$$

where $V_x(0)$ $[m/s]$ and $V_x$ $[m/s]$ are the speed at the start and end of the discretization interval respectively. Eq. 5 and Eq. 4 can be used to compute the vehicle speed $V_x$. However, Eq. 4 requires a definition of the average air drag force and it is still dependent on the time interval $\Delta t$. An analytical expression for $\bar{F}_{drag}$ is introduced to reduce the error in $\Delta V_x$-estimation. Such an error would occur if $F_{drag}$ is calculated only using the speed at the start of the discretization interval. These final two steps (i.e. air drag definition and time interval dependency removal), which result in an expression for $\Delta V_x$ are explained in the following paragraphs.

**Average air drag computation:** the average air drag force is computed assuming a linear increase in vehicle speed during the discretization interval:

$$V_x(t) = V_x(0) + \frac{\Delta V_x}{\Delta t}t. \quad (6)$$

Furthermore, the average air drag is defined as the time integral of air drag, divided by the length of the time interval:

$$\bar{F}_{drag} = \frac{1}{\Delta t}\int_0^{\Delta t} C_dAV_x^2(t)dt. \quad (7)$$

Substitution of Eq. 6 in Eq. 7 and solving the integral yields:

$$\bar{F}_{drag} = C_dA\left(V_x^2(0) + \Delta V_x V_x(0) + \frac{1}{3}\Delta V_x^2\right). \quad (8)$$

Note that Eq. 8 has no dependency on $\Delta t$.

**Time interval dependency removal:** to move the discretization of Eq. 4 from the time to the distance domain, consider the average speed $\bar{V}_x$ as:

$$\bar{V}_x = \frac{\Delta s}{\Delta t} = \frac{\Delta V_x}{2} + V_x(0),$$

which can be rearranged to an expression for $\Delta t$:

$$\Delta t = \frac{2\Delta s}{2V_x(0) + \Delta V_x}. \quad (9)$$

**Computation of the speed increase:** finally, replacing Eq. 8 and Eq. 9 into Eq. 4 yields:

$$\left(\frac{m}{2\Delta s} + \frac{1}{3}C_dA\right)\Delta V_x^2 + V_x(0)\left(\frac{m}{\Delta s} + C_dA\right)\Delta V_x = F_x - C_dAV_x(0)^2 - mg(c_{rr}cos\alpha + sin\alpha) \quad (10)$$

Under the assumption of a linear speed increase, Eq. 10 is a quadratic equation in $\Delta V_x$ independent of $\Delta t$. As a result, solving for $\Delta V_x$ and replacing the result in Eq. 6 provides the means to compute the future speed of the vehicle.

**Cost definition:** the cost function is defined as:

$$C = f(F_x, V_x) = \sum_{i=1}^{N} P_{batt}\left(F_x(i), V_x(i)\right)\Delta t(i) + \sum_{i=1}^{N} \beta \Delta t(i), \quad (11)$$

where $\beta$ is a tuning parameter, $\Delta t(i)$ the time interval needed to move one step in the prediction, and $N$ the control horizon. The cost function consist of the discrete time integral of the battery power and a term controlled by a $\beta$ that penalizes slow driving. The optimization problem is defined as follows:

$$\begin{aligned} \min_{F_x} \quad & C \\ \text{s.t.} \quad & \underline{V}_x(s(i)) \leq V_{x,i}(s(i)) \leq \overline{V}_x(s(i)) \\ & \underline{P}_n(V_x) \leq P_n \leq \overline{P}_n(V_x), \end{aligned} \quad (12)$$

where $s(i)$ represents the distance in the location $i$. As can be seen from Eq. 12, the control problem is subject to the following constraints:

- Minimum and maximum speed $\underline{V}_x$ and $\overline{V}_x$: as mentioned previously, the speed constraints are provided on a distance-based, since legal traffic speed limits are based on the location of the vehicle. These limitations are implemented as hard constraints.
- Minimum and maximum power constraints $\underline{P}_n$ and $\overline{P}_n$: the powertrain components such as electric motor and battery are limited in terms of minimum and maximum power. In this constraint, $n$ refers to each of the powertrain components such as electric motor and battery. These limitations are implemented as hard constraints. Note that e.g. a motor torque constraint can be reformulated as a speed-dependent power constraint, hence the notation in Eq. 12.
- Average speed: a soft constraint on average speed is added to the cost function in Eq. 11. This constraint ensures that the vehicle does not slow down surrounding traffic. Because an additional distance state would be needed to enforce a hard constraint on average speed (i.e. requiring a minimum travelled distance over the horizon), a soft constraint is used instead. This constraint is controlled using $\beta$.

### *3.2 Thermal optimization*

The state dynamics for cabin temperature are given by differential Eq 3. The objective function of the thermal optimization is then defined as minimizing the battery energy consumption over the control horizon via optimization of the HVAC input power:

$$\begin{aligned} \min_{T_{inlet}(t)} \quad & \int_0^t P_{batt}\left(P_{\text{HVAC}}(t), P_{wh}(t)\right) dt \\ \text{s.t.} \quad & \underline{T}_{cab} \leq T_{cab} \leq \overline{T}_{cab} \\ & \underline{T}_{inlet} \leq T_{inlet} \leq \overline{T}_{inlet} \end{aligned} \quad (13)$$

As previously mentioned, the sign convention is chosen such that a positive power flow discharges the battery. $P_{wh}$ represents the power demand at the wheel that follows from the speed optimization (see Figure 1). $P_{\text{HVAC}}$ is defined in Table 1.

The optimization is subject to constraints on the maximum and minimum cabin temperature ($\overline{T}_{cab}$,$\underline{T}_{cab}$), as well as constraints on maximum and minimum cabin air inlet temperature ($\overline{T}_{inlet}$,$\underline{T}_{inlet}$). The maximum and minimum cabin temperatures are set to provide a thermal comfort zone for the driver, while allowing a buffer for the optimizer to store or release energy in form of temperature.

## 4. SIMULATION RESULTS

This section provides with a set of simulations that show the potential energy savings of the proposed PEMS.

The PEMS is simulated using Matlab/Simulink. The parameters of a passenger BEV from Table 2 are used. The controller parameters are $\Delta_s = 10m$, $\beta = XX$, and $N = 20$ (i.e., $2000m$). For the speed advisor, the speed limit depends on the upcoming route, therefore varies between $\overline{V}_x(s(i)) = 50\ km/h$ and $\overline{V}_x(s(i)) = 100\ km/h$, as shown in the next section. The constraints for the thermal optimizer are $\underline{T}_{cab} = 21°C$, $\overline{T}_{cab} = 23°C$, $\underline{T}_{inlet} = -10°C$, and $\overline{T}_{inlet} = 40°C$. The optimal control problem is solved using a DP algorithm, written in C and implemented via a Simulink S-function. The algorithm is implemented in a computer with an *Intel i7* 4th generation processor and 16 GB of RAM memory. The resulting algorithm runs faster than real time. The PEMS is compared to a baseline strategy, which uses Proportional Integral (PI) control for speed and/or thermal management system. The speed PI controller follows the traffic flow as a reference. The thermal PI controller follows a reference equal to the average temperature of the DP algorithm (within the comfort zone of the driver). Both PI controllers were tuned via trial-error to obtain the best performance with reasonable system responses. The controllers are tested using two drive cycles, one showing more frequent changes of speed limit than the other. The results with each drive cycle are explained in the next subsections. Energy savings $\Delta E_{batt}$ are computed using the consumed battery energy with PI and PEMS strategies, i.e.

$$\Delta E_{batt}[kWh] = E_{batt,PI}[kWh] - E_{batt,PEMS}[kWh]$$

$$\Delta E_{batt}[\%] = \frac{E_{batt,PI}[kWh] - E_{batt,PEMS}[kWh]}{E_{batt,PI}[kWh]} \times 100,$$

where $E_{batt,PEMS}[kWh]$ and $E_{batt,PI}[kWh]$ are the consumed battery energy with the PEMS and PI controller, respectively.

### *4.1 Simulation results for cycle with frequent change of speed limit*

This cycle shows a large number of speed changes in order to demonstrate the benefit of using preview information for energy savings of the predictive algorithms.

Fig 3 shows the response of the speed profile when using the developed PEMS compared to the baseline strategy. It is noted that the PEMS uses DP for both speed and thermal system, while the baseline strategy uses PI control for speed and DP for the thermal system. To make a fair comparison, the final average speed is virtually the same at the end of the experiment. At the beginning of the experiment, the PEMS goes to speed limit, while PI controller goes with the average traffic flow. Because of

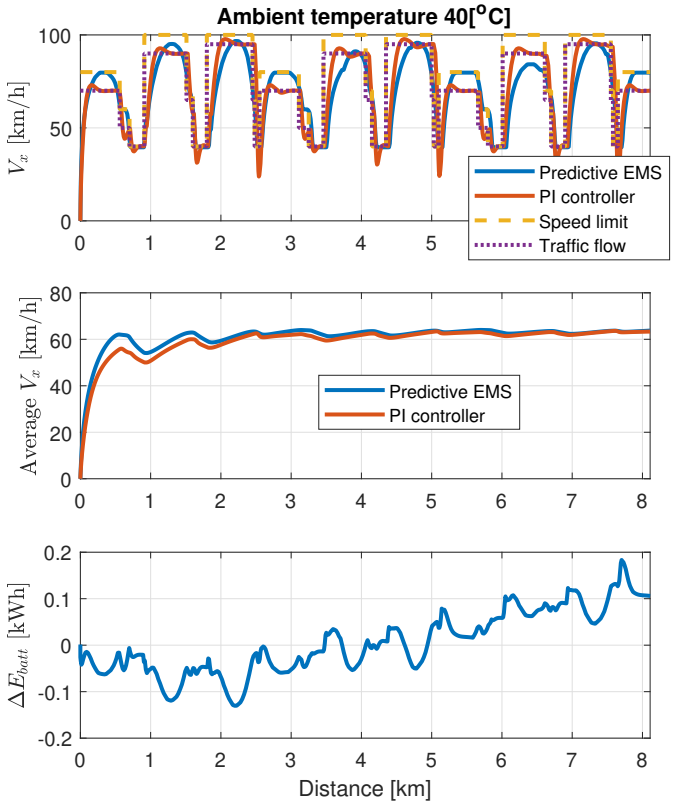


Fig. 3. Comparison of speed profile generation strategies.

this response, there are initially no energy savings, i.e. $\Delta E_{batt} < 0$. However, due to the multiple speed changes, the PEMS achieves a smoother speed profile, which results in an increase of savings compared to the PI controller.

Fig 4 shows the effect of the PEMS of the HVAC. To make a fair comparison, the final average cabin temperature ($\bar{T}_{cab}$) is virtually the same at the end of the experiment. The speed profile is kept the same in order to make a fair comparison between controllers. The PEMS shows positive energy savings during the whole experiment (i.e. $\Delta E_{batt} > 0$). The figure also shows that the there are peaks of power consumption in the HVAC (i.e. the HVAC is activated) every-time that the vehicle is regenerating energy from the brakes. This allows to directly consume the braking energy in cooling the cabin, rather than storing it in the battery for later use. The energy savings are generated by this process.

Table 3 shows the effect of each PEMS on energy savings over multiple ambient temperatures. The column titled "thermal PEMS" presents the energy savings, when PEMS is used for the thermal system while PI control is used for the speed. Likewise, the column titled "speed PEMS" presents the energy savings, when the PEMS is used for speed while a PI control is used for thermal system. The column called "multi-layer PEMS" shows the energy savings of using PEMS for both speed and thermal optimization, compared to the baseline strategy. In Table 3, energy savings of the PEMS in the HVAC (column Thermal PEMS $\Delta E_{HVAC}$ [%]), range from 12 to 41%. This is reflected on battery savings ranging from 1.1 to 1.6%. One can observe that using PEMS of the thermal system helps to reduce the energy consumption of the

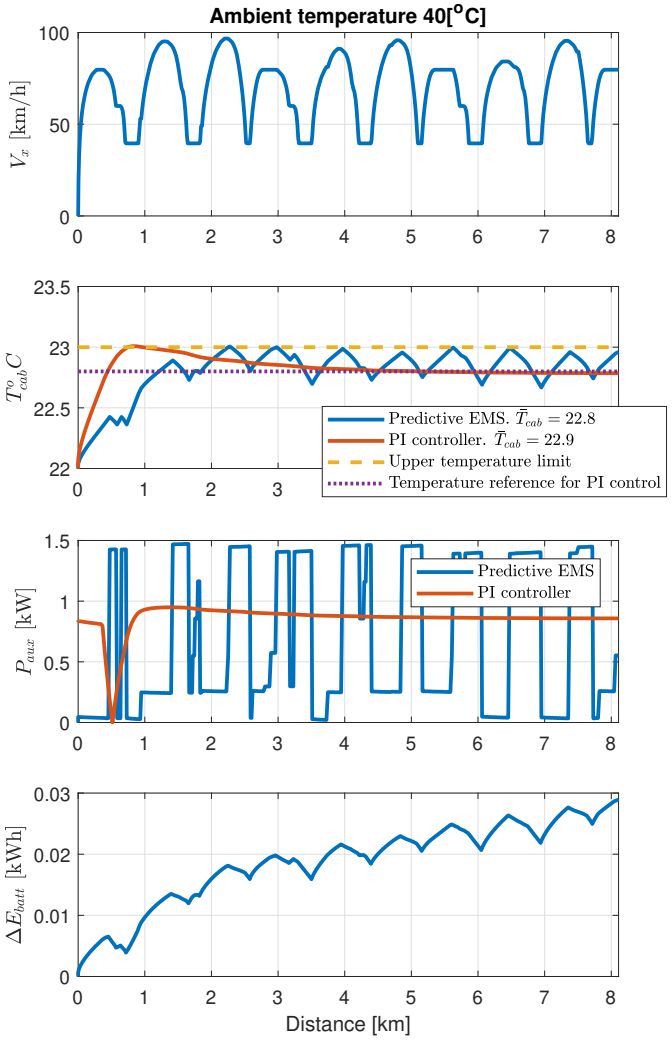


Fig. 4. Comparison of thermal management strategies. The speed profile is generated with the predictive EMS on both controllers. $\bar{T}_{cab}$ is the average cabin temperature.

HVAC which ultimately contributes to the reduction of the battery energy. The table also shows that the thermal PEMS shows potential energy savings across the multiple ambient temperatures considered in the experiment. It can also be noticed that when using the multi-layer PEMS, the energy savings of the individual thermal and speed optimization roughly result in the total savings of the multi-layer strategy. Therefore, adding multiple layers is beneficial to the total energy savings of the vehicle.

### *4.2 Simulation results for cycle with little change on maximum speed limit*

The aforementioned controllers were also tested on a real drive cycle. Such cycle corresponds to the road from the Automotive campus in the city of Helmond to the city centre of Helmond. Compared to the previous drive cycle, Helmond drive cycle does not include significant speed changes while the road elevation is virtually zero. The results of Helmond drive cycle are shown in Table 4, which follows the same conditions of Table 3.

Table 3. Effect of PEMSs on energy savings. The comparison is made with a PI control using the generated cycle. Temperature effect is also shown. $\Delta E_{HVAC}$ is computed in the same way as $\Delta E_{batt}$ but considering HVAC power consumption instead.

| $T_{amb}$ | Thermal PEMS | | Speed PEMS | Multi-layer PEMS savings [%] |
|---|---|---|---|---|
| | $\Delta E_{HVAC}$ [%] | $\Delta E_{batt}$ [%] | $\Delta E_{batt}$ [%] | |
| -10 | 21.65 | 1.3 | 5.6 | 6.9 |
| 0 | 41.1 | 1.6 | 5.7 | 7.3 |
| 20 | 35.95 | 1.1 | 5.6 | 6.8 |
| 30 | 21.75 | 1.5 | 5.6 | 7.2 |
| 40 | 12.95 | 1.5 | 5.6 | 7.1 |

Table 4. Effect of PEMSs on energy savings. The comparison is made with a PI control using the cycle from Helmond. Temperature effect is also shown.

| $T_{amb}$ | Thermal PEMS | | Speed PEMS | Multi-layer PEMS savings [%] |
|---|---|---|---|---|
| | $\Delta E_{HVAC}$ [%] | $\Delta E_{batt}$ [%] | $\Delta E_{batt}$ [%] | |
| -10 | 11.3 | 1.1 | 0.4 | 1.6 |
| 0 | 25.15 | 1.5 | 0.6 | 2.1 |
| 20 | 38.05 | 1.6 | 0.6 | 2.3 |
| 30 | 14.55 | 1.25 | 0.55 | 1.8 |
| 40 | 8 | 1 | 0.5 | 1.6 |

Table 4 shows that the speed optimization have lower energy savings in the Helmond drive cycle. This is because the fewer speed changes give less room to save power by generating an optimal speed profile that reduces losses in the powertrain. Therefore, the savings of the speed PEMS are more significant when frequent changes on speed are required. Once again, savings are observed across all the tested ambient temperatures. Likewise, the individual savings of each layer of the PEMS are virtually added to the total savings of the multi-layer PEMS.

## 5. CONCLUSIONS

A multi-layer Predictive Energy Management System (PEMS) for Battery Electric Vehicle (BEV) has been presented, which consists of two layers. The first layer generates a speed profile (i.e. speed optimization) that minimizes driving energy. The second layer minimizes the total battery energy consumption produced by the Heating, Ventilation, and Air Conditioning (HVAC) system (i.e. thermal optimization). Simplified powertrain and vehicle models are used to accelerate the optimization algorithm inside of each PEMS layer.

Simulations are used to compare the savings of individual PEMS layers (i.e. either speed or thermal optimization), the multi-layer PEMS, and a baseline PI strategy for speed and/or thermal control. Each individual PEMS layer and the multi-layer PEMS show energy savings when compared to the baseline controller. Evaluating the performance of only the thermal optimization shows that the thermal PEMS saves energy even when multiple ambient temperatures are considered. Likewise, evaluating the energy savings of only the speed PEMS shows that savings depend on the amount of speed changes forced by the road profile: more speed changes potentially results in more energy savings. Moreover, the individual savings of each PEMS layer, virtually adds up to the total savings of multi-layer PEMS.

As future work is considered to explore theoretical aspects such as including uncertainty in traffic conditions into the PEMS, as well as more practical aspects such as the driver satisfaction while using the multi-layer PEMS.

## ACKNOWLEDGEMENTS

**This project has received funding from the European Union's Horizon 2020 research and innovation program under Grant Agreement no. 769935.**

## REFERENCES

Cao, J., Schofield, N., and Emadi, A. (2008). Battery balancing methods: A comprehensive review. In *2008 IEEE Vehicle Power and Propulsion Conference*, 1–6.

de Santiago, J. et al. (2012). Electrical motor drivelines in commercial all-electric vehicles: A review. *IEEE Transactions on Vehicular Technology*, 61(2), 475–484.

Eckstein, J. et al. (2016a). A comparison of two predictive approaches to control the longitudinal dynamics of electric vehicles. *Procedia Technology*, 26, 465 – 472. 3rd International Conference on System-Integrated Intelligence: New Challenges for Product and Production Engineering.

Eckstein, J. et al. (2016b). A novel approach using model predictive control to enhance the range of electric vehicles. *Procedia Technology*, 26, 177 – 184. 3rd International Conference SysInt.

Egbue, O. and Long, S. (2012). Barriers to widespread adoption of electric vehicles: An analysis of consumer attitudes and perceptions. *Energy Policy*, 48, 717 – 729. Special Section: Frontiers of Sustainability.

Guzzella, L., Sciarretta, A., et al. (2007). *Vehicle propulsion systems*, volume 1. Springer.

Morlock, F., Heppeler, G., et al. (2017). Range extension for electric vehicles by optimal velocity planning considering different driver types. In *IEEE CCTA*, 554–559.

Onat, N. (2015). *A macro-level sustainability assessment framework for optimal distribution of alternative passenger vehicles*. University of Central Florida.

Pham, T.H., Kessels, J.T.B.A., et al. (2016). Analytical solution to energy management guaranteeing battery life for hybrid trucks. *IEEE Transactions on Vehicular Technology*, 65(10), 7956–7971.

Schaut, S. and Sawodny, O. (2019). Thermal management for the cabin of a battery electric vehicle considering passengers' comfort. *IEEE Transactions on Control Systems Technology*, 1–17.

Yan, Q., Zhang, B., and Kezunovic, M. (2014). Optimization of electric vehicle movement for efficient energy consumption. In *2014 North American Power Symposium (NAPS)*, 1–6.

Zhang, Z., Li, W., Zhang, C., and Chen, J. (2017). Climate control loads prediction of electric vehicles. *Applied Thermal Engineering*, 110, 1183 – 1188.